

VeLU: Variance-enhanced Learning Unit for Deep Neural Networks

Ashkan Shakarami^{1,2*}, Yousef Yeganeh³, Azade Farshad³, Lorenzo Nicolè²,
Stefano Ghidoni², Nassir Navab³

¹University of Bonn, Germany

²University of Padova, Italy

³Technical University of Munich, Germany

{ashkan.shakarami, lorenzo.nicole}@phd.unipd.it, stefano.ghidoni@unipd.it

{y.yeganeh, azade.farshad, nassir.navab}@tum.de

Abstract

Activation functions play a critical role in deep neural networks by shaping gradient flow, optimization stability, and generalization. While ReLU remains widely used due to its simplicity, it suffers from gradient sparsity and dead-neuron issues and offers no adaptivity to input statistics. Smooth alternatives such as Swish and GELU improve gradient propagation but still apply a fixed transformation regardless of the activation distribution. In this paper, we propose **VeLU**, a Variance-enhanced Learning Unit that introduces variance-aware and distributionally aligned nonlinearity through a principled combination of ArcTan-ArcSin transformations, adaptive scaling, and Wasserstein-2 regularization (Optimal Transport). This design enables VeLU to modulate its response based on local activation variance, mitigate internal covariate shift at the activation level, and improve training stability without adding learnable parameters or architectural overhead. Extensive experiments across six deep neural networks show that VeLU outperforms ReLU, ReLU6, Swish, and GELU on 12 vision benchmarks. The implementation of VeLU is publicly available in [GitHub](#).

Keywords: Activation function, Adaptive scaling, Variance-aware learning, Gaussian distribution, Optimal transport.

*Corresponding author: ashkan.shakarami@uni-bonn.de, ashkan.shakarami.ai@gmail.com

1 Introduction

Activation functions are key building blocks in deep neural networks, as they determine the stability of training, the effectiveness of gradient propagation, and the model’s ability to generalize. The Rectified Linear Unit (ReLU) [1, 2] remains widely used due to its simplicity and computational efficiency. However, ReLU suffers from the dying-neuron problem, where units with persistently negative preactivations stop contributing gradients during training. Several variants such as Leaky ReLU [3], PReLU [72], and ELU [4] alleviate this limitation by allowing non-zero gradients for negative inputs.

More recent activation functions, including Swish [18] and GELU [5], introduce smooth, non-monotonic behavior and improve gradient flow. However, these functions apply a fixed transformation independent of the statistical properties of the input, limiting their adaptability across layers where activation distributions may vary considerably. Adaptive activation approaches such as Dynamic ReLU [73] attempt to address this through input-conditioned or learnable parameters, but at the cost of increased architectural or computational overhead.

Although numerous variants of ReLU, Swish, and adaptive nonlinearities have been proposed [8, 18], a

key open question remains: *can we design an activation function that provides adaptivity, non-linearity, and distributional stability - without adding trainable parameters or modifying model architecture?* To this end, we introduce VeLU, a Variance-enhanced Learning Unit that adaptively modulates its response based on the local variance of input activations, enabling data-dependent nonlinearity while preserving the plug-and-play nature of standard activation layers.

Unlike conventional activation functions, VeLU directly mitigates internal covariate shift [9] by incorporating variance-aware scaling and distributional alignment at the activation level, rather than relying on batch-wide or feature-wide normalization statistics. This property enhances training stability in deep Convolutional Neural Networks (CNNs) and Vision Transformers (ViTs), where activation distributions can drift substantially during optimization.

The design of VeLU is grounded in a principled composition of smooth transformations. The ArcTan-ArcSin component introduces controlled curvature and bounded non-linearity, improving gradient behavior while avoiding saturation. A variance-based modulation term dynamically scales the activation based on local activation statistics, enabling continuous adaptivity without requiring additional learnable parameters. Finally, a Wasserstein-2 regularization component, inspired by Optimal Transport theory [11, 15, 16], softly aligns activation outputs with a target Gaussian distribution, stabilizing representation dynamics and reducing activation drift (While OT-based methods have been widely used in generative modeling and domain adaptation [29], their integration into activation design remains largely unexplored).

Extensive experiments on CIFAR-10, CIFAR-100, MNIST, Fashion-MNIST, Corel-1K, and Corel-10K, PathMNIST, BloodMNIST, PACS, EuroSAT-RGB, Oxford-IIIT Pet, and Tiny-ImageNet demonstrate that VeLU consistently improves performance across six architectures, including ViT-B16, VGG19, ResNet50, DenseNet121, MobileNetV2, and EfficientNetB3 [12, 13, 47, 46, 52]. These results position VeLU as an effective, architecture-agnostic, and computationally lightweight alternative to conventional

activation functions for deep neural networks.

2 VeLU

2.1 Structure

Mathematically, VeLU is defined in Equation 1, where $\sigma(x)$ denotes the sigmoid function and λ is a trainable scaling parameter. The hyperparameters α , β_1 , β_2 , γ , μ , the momentum term m , and the Wasserstein weight λ_{OT} jointly govern the curvature, adaptivity, and distributional behavior of the activation. Importantly, VeLU adds no new layers and only one trainable scalar (λ), preserving the architectural simplicity of standard activation layers while enabling variance-aware modulation. In the following, we provide a detailed description and motivation for each component.

$$f(x) = \lambda \cdot x \cdot \sigma(\alpha [\tan^{-1}(\beta_1 x) + \sin^{-1}(\beta_2 x)]) \times (1 + \gamma \tanh(m \mu \sigma_x)) - \lambda_{OT} \cdot W_2(x, \mathcal{N}(0, 1)). \quad (1)$$

Motivation for the components. Following the design rationale, each term plays a specific role:

- Scaling factor λ :**
 A learnable scalar that lets the network adjust the global amplitude of the activation to compensate for the composite transformation.
- Base term x :**
 Maintains an identity-like behavior near the origin, preserving gradient flow when inputs are small.
- ArcTan-ArcSin composite:**
 $\sigma(\alpha(\tan^{-1}(\beta_1 x) + \sin^{-1}(\beta_2 x)))$ provides smooth, bounded non-linearity. The combination of \tan^{-1} and \sin^{-1} yields gradual saturation and symmetric curvature, mitigating abrupt plateaus seen in hard-saturating or piecewise-linear units. Scaling Parameter α controls the strength of the non-linearity by scaling the ArcTan-ArcSin argument before the sigmoid. Larger α increases

curvature and sharp transitions; smaller values lead to smoother behavior. Transformation Parameters (β_1 and β_2 scale the inputs to arctan and arcsin, respectively. Larger values accentuate non-linear regions and produce sharper responses; smaller values make the activation more linear. This tunability allows fine-grained control over the shape of the gating non-linearity.

- **Variance-adaptive modulation:**

$1 + \gamma \tanh(m\mu\sigma_x)$ adapts the effective non-linearity to the dispersion of activations. The hyperbolic tangent keeps the factor bounded, while m controls how sensitively this term reacts to changes in σ_x , similar in spirit to a “momentum” on variance. Adaptive scaling factor γ determines how strongly the activation is modulated by variance. Larger γ increases the amplitude of variance-driven adaptation; very large values can over-amplify high-variance regions and thus require care. The momentum hyperparameter m adjusts the sensitivity of the variance-aware scaling to changes in σ_x and acts as a smoothing factor over the batch statistics.

- **Wasserstein-2 regularization:**

$-\lambda_{OT}W_2(x, \mathcal{N}(0, 1))$ softly aligns the activation statistics with a Gaussian target, promoting stability and mitigating activation drift in a geometry-aware way. λ_{OT} controls the contribution of the Wasserstein-2 penalty. Larger λ_{OT} enforces stronger statistical alignment with the Gaussian prior, which can improve stability and generalization but may hamper convergence if chosen too large.

2.2 Visual behavior

Figure 1 compares VeLU with standard activation functions (ReLU, Swish, GELU) over the input interval $[-1.5, 1.5]$. ReLU exhibits a sharp kink at $x = 0$ and zero response for negative inputs, which can lead to dead units. Swish and GELU provide smooth transitions and improved gradient flow, yet they apply a static transformation that does not adapt to activation statistics. In contrast, VeLU

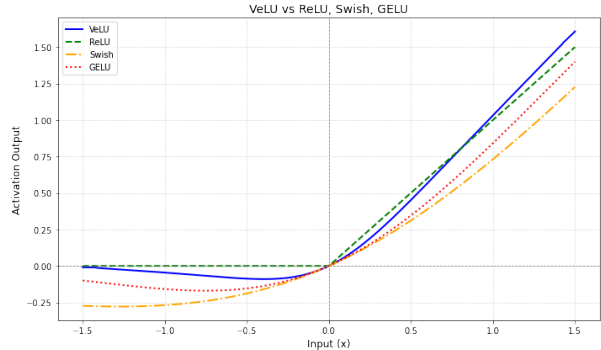


Figure 1: Comparison of VeLU with standard activation functions (ReLU, Swish, GELU) in the range $[-1.5, 1.5]$. The plot highlights smoothness, non-linearity, and the adaptive behavior introduced by VeLU.

maintains smooth, bounded behavior while introducing self-adaptive scaling and distributional regularization via the Wasserstein-2 term. This comparison highlights the foundational curvature and adaptivity advantages of VeLU over traditional activations.

Building on this comparison, Figure 2 visualizes how the internal components of VeLU interact under different configurations of α , β_1 , β_2 , γ , μ , and m . The ArcTan-ArcSin composite governs curvature and smoothness, while the variance-based term (σ_x) dynamically adapts the response to the dispersion of preactivations. Together, these mechanisms yield a richer and more flexible activation landscape than static nonlinearities. The Wasserstein-2 regularization term further encourages the activation outputs to align with a stable Gaussian target, reducing activation drift and mitigating internal covariate shift at the activation level.

2.3 Mathematical characteristics

VeLU exhibits a non-monotonic yet smooth response due to the ArcTan-ArcSin structure. Unlike ReLU, which thresholds negative values at zero, VeLU retains small negative activations, helping to propagate gradients and avoid neuron death.

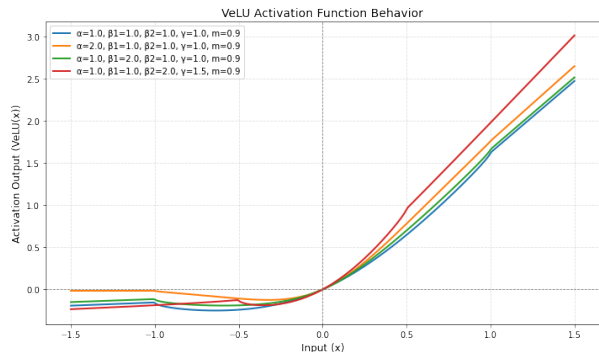


Figure 2: Behavior of VeLU under different parameter configurations. The curves illustrate how curvature, smoothness, and variance-adaptive modulation emerge from the ArcTan-ArcSin composite, scaling term, and Wasserstein alignment.

The variance-based scaling factor is defined as

$$s_{\text{adaptive}} = 1 + \gamma \cdot \tanh(m \cdot \mu \cdot \sigma_x), \quad (2)$$

where σ_x is the standard deviation of preactivations over the mini-batch. This factor adjusts the effective non-linearity according to activation dispersion: for small σ_x , $s_{\text{adaptive}} \approx 1$; for large σ_x , it approaches $1 + \gamma$ (with saturation mediated by $m \cdot \mu$).

To further stabilize training, VeLU incorporates Wasserstein-2 distance minimization between its outputs and a Gaussian target:

$$W_2^2 = (E[x] - \mu)^2 + (\sigma_x - \sigma_{\text{target}})^2, \quad (3)$$

which penalizes deviations in mean and variance, encouraging well-conditioned internal representations.

Figure 3 illustrates the distribution of preactivations before and after training ResNet50 with VeLU. The post-training distribution is more concentrated and symmetric, indicating that VeLU stabilizes activation dynamics and mitigates internal covariate shift.

2.4 Smoothness and Adaptability

Because all components in Equation 1 are smooth, VeLU is continuously differentiable. This con-

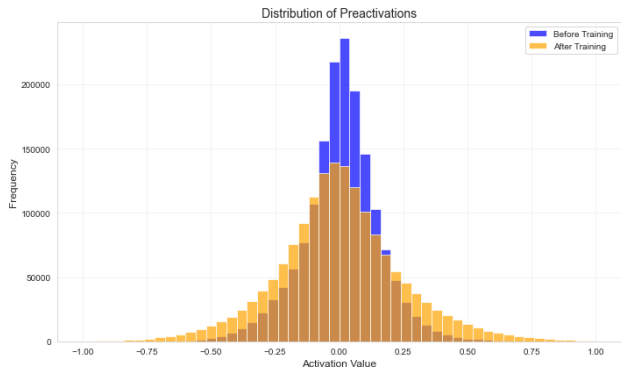


Figure 3: Histogram of preactivation values from a hidden layer in ResNet50, before and after training with VeLU. The post-training distribution is more concentrated and symmetric, reflecting improved activation stability.

trasts with ReLU, which is continuous but non-differentiable at zero. The first derivative of VeLU can be written (in simplified form) as

$$f'(x) = \lambda \sigma'(h(x)) h'(x) s_{\text{adaptive}} + \lambda x \sigma(h(x)) \gamma m \mu \operatorname{sech}^2(m \mu \sigma_x). \quad (4)$$

where $h(x) = \alpha(\tan^{-1}(\beta_1 x) + \sin^{-1}(\beta_2 x))$, and $\sigma'(h(x)) = \sigma(h(x))(1 - \sigma(h(x)))$. The $\operatorname{sech}^2(\cdot)$ term arises from the derivative of the $\tanh(m \mu \sigma_x)$ in Equation 2; in practice, σ_x is treated as slowly varying within a batch, making this expression a good approximation of the gradient behavior. This derivative shows that VeLU maintains non-zero gradients across a broad activation range, avoiding the sharp gradient sparsity seen in ReLU and the rapid saturation of sigmoid/tanh. The resulting loss landscape is smoother and better conditioned, as visualized in Figure 4, which improves optimization stability in deep networks.

By dynamically adapting to the input distribution and incorporating Wasserstein-2 regularization, VeLU maintains well-behaved activation distributions throughout training, reduces internal covariate shifts, and more stable convergence, as demonstrated empirically in section 3.

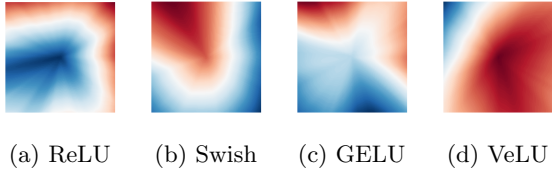


Figure 4: Output landscapes of a randomly initialized ResNet50 with different activation functions. VeLU yields a smoother, variance-adaptive landscape compared to ReLU, Swish, and GELU.

2.5 Parameter Selection and Stability Considerations

The behavior of VeLU is governed by the parameters α , β_1 , β_2 , γ , momentum, and λ_{OT} , each controlling a distinct component of the activation: nonlinearity strength, curvature of the ArcTan-ArcSin transformation, adaptive scaling sensitivity, and regularization intensity. While VeLU is stable under the recommended default configuration, improper parameter scaling may lead to gradient explosion or numerical instability. This section formalizes the conditions under which VeLU behaves reliably.

Nonlinearity parameters (α , β_1 , β_2). Larger values sharpen the composite transformation $h(x) = \alpha(\tan^{-1}(\beta_1 x) + \sin^{-1}(\beta_2 x))$, which increases sensitivity to input variations. However, excessively steep curvature amplifies the term $\sigma'(h(x))h'(x)$ in the gradient, potentially producing exploding updates. To mitigate this, we recommend $0.05 \leq \alpha \leq 0.2$ and $0.05 \leq \beta_1, \beta_2 \leq 0.3$ for stable training across CNNs and ViTs.

Adaptive scaling parameter (γ). The batch-adaptive factor

$$a(x) = 1 + \gamma \cdot \tanh(\text{momentum} \cdot \sigma_x)$$

modulates the activation shape according to batch dispersion. To avoid excessively large scaling we ap-

ply a clipped form:

$$\text{adapt_factor} = \text{clip}(1 + \gamma \tanh(\text{std.dev} \cdot \text{momentum}), 0.5, 2.0), \quad (5)$$

Experiments show that values $\gamma \leq 0.2$ guarantee smooth adaptation without destabilizing backpropagation.

Numerical stability. The computation

$$\text{std.dev} = (\mathbb{E}[x^2] + \epsilon)^{-1/2}$$

is sensitive to small batch variances; a too-small ϵ produces extreme scaling. We recommend $\epsilon = 10^{-3}$ rather than 10^{-6} .

Wasserstein regularization (λ_{OT}). λ_{OT} controls the strength of distributional alignment to a Gaussian target. Large values bias the activations toward overly constrained distributions and may hinder optimization. Empirically stable regimes [45] lie within $\lambda_{OT} \in [0.001, 0.05]$. If divergence or NaN gradients occur, reducing λ_{OT} immediately stabilizes training.

Practical guidelines. To ensure stable optimization across all architectures, we recommend:

- Use gradient clipping (e.g., `clipnorm = 1.0`).
- Use $\epsilon = 10^{-3}$ in variance computations.
- Clamp the adaptive scaling factor to $[0.5, 2.0]$.
- Reduce λ_{OT} when facing divergence.

These recommendations establish a principled and reproducible parameter regime for VeLU.

2.6 Extended Theoretical Properties of VeLU

This section formalizes the differentiability, adaptive behavior, and regularization properties of VeLU.

2.7 Definition

For an input $x \in \mathbb{R}$, VeLU is defined as:

$$\text{VeLU}(x) = \lambda x \sigma(h(x)) a(x) - \lambda_{OT} W_2,$$

where σ is the sigmoid function, $h(x)$ is the composite transformation, $a(x)$ is the adaptive scaling term, and W_2 is the empirical Wasserstein-2 alignment penalty.

$$\begin{aligned} h(x) &= \alpha [\tan^{-1}(\beta_1 x) + \sin^{-1}(\beta_2 x)], \\ a(x) &= 1 + \gamma \tanh(m \sigma_x). \end{aligned} \tag{6}$$

2.7.1 Gradient

Using the product rule:

$$\begin{aligned} \frac{\partial \text{VeLU}}{\partial x} &= \lambda [\sigma(h(x)) + x \sigma'(h(x)) h'(x)] a(x) \\ &+ \lambda x \sigma(h(x)) a'(x) - \lambda_{OT} \frac{\partial W_2}{\partial x}. \end{aligned} \tag{7}$$

with:

$$h'(x) = \alpha \left(\frac{\beta_1}{1 + (\beta_1 x)^2} + \frac{\beta_2}{\sqrt{1 - (\beta_2 x)^2}} \right).$$

All components are smooth on their respective domains, ensuring $\text{VeLU} \in \mathcal{C}^1(\mathbb{R})$.

2.7.2 Adaptive Scaling Interpretation

The scaling term satisfies:

$$\lim_{\sigma_x \rightarrow 0} a(x) = 1, \quad \lim_{\sigma_x \rightarrow \infty} a(x) = 1 + \gamma.$$

Thus VeLU increases nonlinearity in high-variance regimes while reducing curvature in low-variance regimes, providing stable and context-aware activation shaping.

2.7.3 Wasserstein Alignment

The OT regularizer minimizes:

$$W_2^2(\mathbb{P}_x, \mathcal{N}(0, 1)) = \mathbb{E} \|x - T(x)\|^2,$$

where T is the optimal transport map. This encourages stable, Gaussian-like activation distributions, reducing internal covariate shift and improving generalization.

These properties together ensure that VeLU maintains smooth gradients, adapts dynamically to feature statistics, and regularizes activations through principled distributional alignment.

2.8 Component-wise Functional Roles

To understand the functional contribution of each design element in VeLU, we conceptually isolate the individual components and examine their theoretical role in shaping the activation behavior. The base multiplicative term x preserves identity-like behavior near the origin and ensures that gradient flow is not hindered for small inputs. Adding the ArcTan-ArcSin composite introduces smooth, bounded curvature that enhances non-linearity while avoiding the abrupt saturation typical of hard-threshold functions.

Incorporating the variance-adaptive scaling term enables the activation to modulate its effective shape in response to the dispersion of preactivations, making VeLU sensitive to local activation statistics without introducing additional learnable parameters. Finally, the Wasserstein-2 regularization term aligns the activation’s output distribution with a stable Gaussian target, reducing activation drift and promoting well-conditioned feature representations throughout training.

Together, these components form a progressively refined activation mechanism: the ArcTan-ArcSin structure shapes the non-linearity, the adaptive scaling provides data-dependent flexibility, and the OT regularization contributes distributional stability. The full VeLU formulation therefore integrates curvature, adaptivity, and statistical alignment into a unified activation framework.

3 Experiments

We evaluated VeLU by comparing it with standard activation functions, including ReLU [1], Swish [18, 36], ReLU6 [30], and GELU [5, 7], across multiple

deep learning architectures and image benchmarks. Unless otherwise stated, we kept all training hyperparameters (optimizer, learning rate schedule, batch size, and data augmentation) identical across activations. Key experiments were repeated with multiple random initializations, and we report mean performance; variance statistics are provided in the supplementary material.

We considered two integration scenarios: (1) *partial replacement* of activation functions and (2) *full replacement* of a model’s activation functions with VeLU. In the first scenario, VeLU was used only in the classification head (the final layers), while the feature extraction backbone retained its original activations. This setup assesses compatibility with existing backbones and is particularly relevant for fine-tuning pre-trained models [27]. Most experiments, including the architectural and benchmark comparisons, follow this scenario. In contrast, the experiments in Table 5 and Table 6, as well as the results summarized in Table 3 and Figure 5, implement the second scenario, where all activation functions in ResNet50 [6] (backbone and added layers) are replaced by VeLU. This demonstrates that VeLU can serve as the primary activation function in a network without relying on additional nonlinearities.

For convolutional models (e.g., ResNet [6], VGG [28], MobileNet [30], and DenseNet [13]), we used a global average pooling layer [31] before the classifier. For ViT_B16 [7], which outputs a 2D feature vector, we omitted pooling. The classifier head consisted of two fully connected layers with 256 and 64 neurons, each followed by an activation function, and a final softmax layer. This standardized design enables a fair comparison of activations across architectures with different inductive biases.

We conducted experiments on CIFAR-10 and CIFAR-100 [32], MNIST [33], Fashion-MNIST [34], Corel-1K, and Corel-10K [35]. Although these benchmarks are relatively classical, they remain standard for evaluating activation functions due to their controlled complexity, ease of reproducibility, and broad adoption in related work. Notably, recent activation proposals such as Swish [18] and GELU [5] also rely on these datasets, enabling meaningful comparisons.

For CIFAR, MNIST, and Fashion-MNIST, we fol-

lowed the original training/validation splits of the benchmarks. For Corel-1K and Corel-10K, we randomly divided the data into 80% training and 20% test sets. Each model was trained for 5-20 epochs, depending on network depth and convergence, and we report mean top-1/top-5 accuracy, loss, training time, inference throughput (FPS), and memory usage.

Although we provide default initialization values for VeLU in our public implementation¹, these can be adjusted for specific tasks. This flexibility enables task-dependent optimization [57], improved generalization [25], and adaptation to different architectures [36]. However, manual tuning can be time-consuming [58, 59] and computationally demanding [60]. As a direction for future work, we propose integrating automated hyperparameter optimization (e.g., Bayesian optimization [62], gradient-based meta-learning [63], or search frameworks such as Optuna [64], Hyperopt [65], and KerasTuner [66]) to set suitable initial values based on sampled data, thereby improving usability and reducing the need for manual tuning.

3.1 Evaluation Across Architectures

Table 1 compares VeLU with standard activation functions across a range of architectures, including CNNs [33, 2, 48] and ViTs [7]. Across all models in this setting (partial replacement in the classifier head), VeLU achieves higher top-1 accuracy than the corresponding baseline activation, confirming its adaptability to both convolutional and transformer-based designs.

Performance gains are particularly pronounced in deeper or residual networks such as ResNet50 and DenseNet121, where VeLU improves top-1 accuracy by nearly 2%, suggesting better gradient flow and more stable optimization. In lightweight architectures like MobileNetV2, the gains are smaller but still positive, indicating suitability under parameter- and compute-constrained conditions. ViT-B16 also benefits: VeLU slightly outperforms GELU in both top-1 and top-5 accuracy, showing compatibil-

¹<https://github.com/AshkanShakarami/Velu>

Table 1: Architectural performance with and without VeLU (partial replacement). Top-1 and Top-5 accuracy (%).

Model	Act.	Top-1	Top-5
EffNetB3	VeLU	87.61	99.40
	Swish	87.18	99.22
VGG19	VeLU	90.97	99.71
	ReLU	90.30	99.82
ResNet50	VeLU	91.27	99.41
	ReLU	89.44	99.61
MobileNetV2	VeLU	91.32	99.70
	ReLU6	90.69	99.77
DenseNet121	VeLU	91.85	99.49
	ReLU	89.99	99.38
ViT-B16	VeLU	96.25	99.95
	GELU	95.80	99.87

ity with self-attention mechanisms and LayerNorm-based pipelines. These trends indicate that VeLU delivers generalizable improvements across architectures with different depth, connectivity, and inductive biases, supporting its role as a plug-in alternative to standard activations.

3.2 Evaluation Across Benchmarks

Table 2 compares MobileNetV2 [12] with and without VeLU across 12 datasets. Integrating VeLU consistently improves top-1 accuracy, with the largest gains observed on CIFAR-100 and the Corel datasets, which involve more classes and higher intra-class variability.

In CIFAR-100 and Corel-10K, VeLU improves both top-1 and top-5 accuracy, indicating better feature discrimination in more complex classification settings. On simpler benchmarks such as MNIST and Fashion-MNIST, where baseline performance is already near-saturated, the improvements are smaller but still positive in top-1 accuracy. Overall, these results show that VeLU enhances performance across tasks of varying complexity.

Table 3 reports top-1 accuracy for ResNet50 [6]

Table 2: MobileNetV2 performance with and without VeLU (partial replacement). Top-1 and Top-5 accuracy (%).

Benchmark	Model	Top-1	Top-5
CIFAR-10	Baseline	90.69	99.77
	VeLU	91.32	99.70
CIFAR-100	Baseline	71.05	91.54
	VeLU	72.63	92.36
MNIST	Baseline	99.01	99.99
	VeLU	99.21	100
Fashion-MNIST	Baseline	91.10	99.75
	VeLU	91.13	99.50
Corel1K	Baseline	91.00	99.00
	VeLU	93.50	100
Corel10K	Baseline	86.45	95.70
	VeLU	87.90	97.50

Table 3: ResNet50 performance with full VeLU activation replacement (Scenario 2). Accuracy and absolute gains.

Benchmark	Acc (%)	Gain
CIFAR-10	91.29	+1.90
CIFAR-100	72.07	+3.12
MNIST	99.34	+0.36
Fashion-MNIST	92.26	+0.66
Corel1K	93.50	+9.00
Corel10K	87.35	+3.85

with full activation replacement by VeLU (Scenario 2), along with the absolute gain over the original activation. Here, VeLU yields consistent improvements across all benchmarks. The largest gains occur on Corel-1K (+9.00%), Corel-10K (+3.85%), and CIFAR-100 (+3.12%), reflecting stronger benefits on more challenging, multi-class datasets. On simpler datasets such as MNIST and Fashion-MNIST, the absolute gains are smaller but still positive.

Figure 5 presents the validation accuracy and loss curves for ResNet50 trained with VeLU compared to ReLU, GELU, and Swish. Already after the first few epochs (around epoch 2-3), VeLU reaches higher val-

idation accuracy than all baselines and maintains this advantage throughout training. This indicates that VeLU not only converges quickly with few epochs, but also preserves a consistent edge in the mid- and late-training phases.

The validation-loss plot shows a similar trend: VeLU exhibits one of the steepest early loss drops and then continues to decrease smoothly, stabilizing at the lowest loss level. In contrast, the losses for ReLU, GELU, and Swish flatten earlier, with ReLU even showing a mild late-epoch increase suggestive of overfitting. These dynamics are consistent with the variance-aware design of VeLU, which supports both fast convergence - beneficial for transfer learning and fine-tuning scenarios - and more stable, well-conditioned optimization in later training stages.

3.3 Training Efficiency and Memory Usage

Table 4 compares activations in terms of final training loss, training time, inference speed, and memory usage (partial replacement scenario). In all convolutional architectures, VeLU achieves lower training loss than the corresponding baseline activation, indicating more effective optimization. In ViT-B16, GELU retains a slightly lower loss, but VeLU remains competitive.

In terms of training time and FPS, VeLU is comparable to the baselines. It is slightly faster in some architectures (e.g., MobileNetV2 and ResNet50) and slightly slower in others (e.g., EfficientNetB3, DenseNet121, ViT-B16), reflecting backend- and architecture-dependent kernel optimizations rather than fundamental complexity gaps. Memory usage with VeLU is also close to that of the baselines, with modest increases in some models due to the additional functional composition.

Overall, Table 4 shows that VeLU delivers consistent gains in training loss and accuracy while maintaining competitive training time, inference throughput, and memory footprint, making it practical for deployment even in resource-constrained settings.

Table 4: Performance of various architectures with and without VeLU. Loss (L), Training Time (T), FPS, and Memory based on Megabyte (M) Usage (MB).

Model	Act.	L	T (s)	FPS	M
EffNetB3	VeLU	0.42	2621.03	16.07	14786
	Swish	0.44	2417.54	15.16	13403
VGG19	VeLU	0.30	2047.57	25.50	14581
	ReLU	0.37	2113.78	28.65	14730
ResNet50	VeLU	0.39	1362.65	20.20	13705
	ReLU	0.53	1353.11	19.76	13119
MobileNetV2	VeLU	0.33	819.40	21.15	14440
	ReLU6	0.37	844.61	16.08	13871
DenseNet121	VeLU	0.32	2246.35	15.78	13628
	ReLU	0.43	1751.09	17.62	13777
ViT-B16	VeLU	0.14	692.38	11.29	13259
	GELU	0.13	676.85	12.33	13554

Table 5: Accuracy of VeLU on CIFAR-10 across different input resolutions using MobileNetV2 (full activation replacement).

Resolution	Top-1	Top-5
32×32	75.10	98.51
64×64	86.51	99.45
128×128	91.32	99.70
224×224	93.34	99.82

3.4 Behavior on Different Image Resolutions

Table 5 reports MobileNetV2 performance with full VeLU replacement on CIFAR-10 at different input resolutions. VeLU maintains stable and improving performance as resolution increases: from 75.10% top-1 accuracy at 32×32 up to 93.34% at 224×224 , with top-5 accuracy consistently above 98.5%. This robustness suggests that VeLU is suitable for settings where input resolution varies, such as transfer learning [36], medical imaging [53, 54], and real-time applications [55].

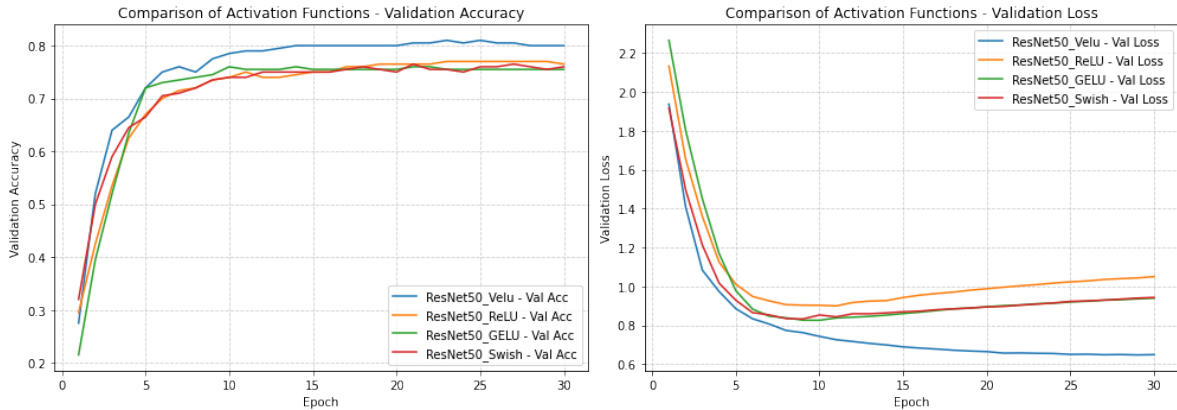


Figure 5: Comparison of VeLU with ReLU, Swish, and GELU in ResNet50. (Left) Validation accuracy: VeLU surpasses all baselines after only a few epochs and keeps a consistent advantage throughout training. (Right) Validation loss: VeLU shows a steep early drop and converges to the lowest loss, whereas the baselines plateau earlier and ReLU exhibits a mild late increase.

Table 6: Accuracy of VeLU as a full replacement for ResNet50 activations on CIFAR-10 across different optimizers at 128×128 resolution.

Optimizer	Top-1	Top-5
Adam	91.32	99.70
SGD	89.33	99.70
Nadam	87.23	99.19
RMSPprop	86.95	99.03

3.5 Adaptability With Different Optimizers

Table 6 evaluates VeLU (full replacement) on ResNet50 with different optimizers on CIFAR-10 at 128×128 resolution. Adam achieves the highest top-1 accuracy (91.32%), but SGD, Nadam, and RMSPprop all maintain high top-5 accuracy, demonstrating that VeLU can be trained effectively under different optimization dynamics. This robustness to optimizer choice is valuable in practice, where the preferred optimizer may depend on computational constraints, convergence behavior, or prior workflow choices [43, 74, 75].

4 Extended Experiments

4.1 Robustness Across Image Resolutions

To evaluate resolution-invariance, we trained MobileNetV2 with VeLU on CIFAR-10 at four input sizes. As shown in Table 5, VeLU maintains stable performance across all resolutions, achieving consistent gains as image size increases. Notably, even at 32×32 resolution - where many adaptive activations underperform - VeLU retains competitive accuracy. This supports our claim that the variance-adaptive scaling mitigates resolution-induced activation drift.

4.2 Optimizer Sensitivity Analysis

We next examined how VeLU interacts with different optimization algorithms. Results for ResNet50 on CIFAR-10 (Table 6) show that VeLU improves performance under all four optimizers tested, with the largest gains under Adam. SGD and RMSPprop also maintain high Top-5 accuracy, confirming that VeLU does not rely on a specific optimizer to achieve stable convergence.

Table 7: Performance comparison of the Baseline (B.) model with and without VeLU in different vision benchmarks. The original Baseline results are referenced from [12].

Benchmark	Model	Top-1	Top-5
PathMNIST [67]	B.	95.01	99.90
	VeLU in B	95.31	99.90
BloodMNIST [67]	B.	96.61	99.94
	VeLU in B.	97.08	100
PACS [68]	B.	97.70	100
	VeLU in B.	98.10	100
EuroSAT-RGB [70]	B.	96.11	99.96
	VeLU in B.	96.43	99.93
Oxford-IIIT Pet [71]	B.	81.92	96.61
	VeLU in B.	83.62	97.77
Tiny-ImageNet [69]	B	69.31	87.12
	VeLU in B.	70.43	87.74

4.3 Evaluation on Additional Benchmarks

To assess generalization across domains and difficulty levels, we evaluated VeLU on medical, satellite, domain-generalization, and fine-grained classification datasets. Shown in Table 7, consistent improvements across PathMNIST, BloodMNIST, PACS, EuroSAT, Oxford-IIIT Pet, and Tiny-ImageNet demonstrate that VeLU enhances learning in both low- and high-variance regimes. Importantly, improvements on medical datasets confirm that the Wasserstein-based alignment stabilizes representations in small-sample settings, while gains on Tiny-ImageNet and Oxford-IIIT Pet indicate improved fine-grained discrimination. Similar neural descriptor stability is critical in CAD systems across neuroimaging and pathology [49, 50, 51].

5 Limitations and Future Work

Limitations. Although the experimental results demonstrate that the proposed activation design achieves consistent improvements across various ar-

chitectures and benchmarks, several limitations remain. First, the current study focuses primarily on medium-scale vision datasets, and large-scale evaluations on more diverse domains are still required to fully assess the activation’s generalizability. Second, while we conducted extensive testing across CNNs and vision transformers, the behavior of the activation in sequence models, multimodal frameworks, and reinforcement-learning settings remains unexplored. Third, our implementation relies on a fixed configuration strategy; a systematic analysis of automatic parameter tuning, stability ranges, and hyperparameter interactions would further clarify the operational boundaries of the method.

Another limitation lies in the scope of ablations: although we investigated the contribution of major components, additional controlled experiments are needed to disentangle interactions between adaptive modulation, normalization aspects, and distributional regularization. Moreover, while computational overhead remains moderate, future work should examine kernel-level optimizations and hardware-specific acceleration for deployment in resource-constrained environments.

Future Work. Alongside extending evaluations to larger datasets and more diverse architectures, we are actively developing an enhanced version of the activation function which incorporates additional mechanisms aimed at improving stability, adaptability, and distributional control without introducing architectural burden. Details of this extension will be presented in a dedicated publication. Beyond this, several research directions appear promising: (i) integrating the activation into foundation models and emerging transformer variants; (ii) exploring its compatibility with low-precision and quantized training; (iii) analyzing theoretical convergence properties under different optimization regimes; and (iv) investigating its role as a building block in self-normalizing or specific training pipelines.

Together, these directions highlight the potential for continued refinement of activation functions that adapt to feature statistics and maintain stable representational dynamics at scale.

6 Conclusion

We introduced VeLU, a variance-aware activation function that combines ArcTan–ArcSin transformations, adaptive scaling, and Wasserstein-2 regularization. Across CNNs and ViTs, VeLU consistently improved accuracy and stability over ReLU, Swish, and GELU, while requiring only a single learnable parameter and minimal computational overhead. Although our experiments focused on medium-scale vision benchmarks, the results indicate that variance-adaptive and distribution-aligned activations are a promising direction. Future work will include large-scale evaluations and exploring VeLU in Transformer-based and sequence models.

References

- [1] V. Nair and G. E. Hinton, “Rectified Linear Units Improve Restricted Boltzmann Machines,” *Proceedings of the 27th International Conference on Machine Learning (ICML)*, pp. 807–814, 2010.
- [2] A. Krizhevsky, I. Sutskever, and G. E. Hinton, “ImageNet Classification with Deep Convolutional Neural Networks,” *Advances in Neural Information Processing Systems (NeurIPS)*, pp. 1097–1105, 2012.
- [3] A. L. Maas, A. Y. Hannun, and A. Ng, “Rectifier Nonlinearities Improve Neural Network Acoustic Models,” in *Proc. ICML Workshop on Deep Learning for Audio, Speech and Language Processing*, 2013.
- [4] D. Clevert, T. Unterthiner, and S. Hochreiter, “Fast and Accurate Deep Network Learning by Exponential Linear Units (ELUs),” *arXiv preprint arXiv:1511.07289*, 2015.
- [5] D. Hendrycks and K. Gimpel, “Gaussian Error Linear Units (GELUs),” *arXiv preprint arXiv:1606.08415*, 2016.
- [6] K. He, X. Zhang, S. Ren, and J. Sun, “Deep Residual Learning for Image Recognition,” *Proceedings of the IEEE Conference on Computer Vision and Pattern Recognition (CVPR)*, pp. 770–778, 2016.
- [7] A. Dosovitskiy et al., “An Image is Worth 16x16 Words: Transformers for Image Recognition at Scale,” *arXiv preprint arXiv:2010.11929*, 2020.
- [8] A. F. Agarap, “Deep Learning using Rectified Linear Units (ReLU),” *arXiv preprint arXiv:1803.08375*, 2018.
- [9] S. Ioffe and C. Szegedy, “Batch Normalization: Accelerating Deep Network Training by Reducing Internal Covariate Shift,” *Proceedings of the 32nd International Conference on Machine Learning (ICML)*, pp. 448–456, 2015.
- [10] P. Wolinski and J. Arbel, “Gaussian Pre-activations in Neural Networks: Myth or Reality?,” *arXiv preprint arXiv:2205.12379*, 2022.
- [11] M. Arjovsky, S. Chintala, and L. Bottou, “Wasserstein Generative Adversarial Networks,” *Proceedings of the 34th International Conference on Machine Learning (ICML)*, pp. 214–223, 2017.
- [12] M. Sandler, A. Howard, M. Zhu, A. Zhmoginov, and L.-C. Chen, “MobileNetV2: Inverted Residuals and Linear Bottlenecks,” *Proceedings of the IEEE Conference on Computer Vision and Pattern Recognition (CVPR)*, pp. 4510–4520, 2018.
- [13] G. Huang, Z. Liu, L. van der Maaten, and K. Q. Weinberger, “Densely Connected Convolutional Networks,” *Proceedings of the IEEE Conference on Computer Vision and Pattern Recognition (CVPR)*, pp. 4700–4708, 2017.
- [14] J. Ba, J. Kiros, and G. Hinton, “Layer Normalization,” *arXiv preprint arXiv:1607.06450*, 2016.
- [15] N. Courty, R. Flamary, A. Habrard, and A. Rakotomamonjy, “Joint Distribution Optimal Transportation for Domain Adaptation,” *Advances in Neural Information Processing Systems (NeurIPS)*, vol. 30, 2017.
- [16] E. F. Montesuma, F. M. N. Mboula, and A. Souloumiac, “Recent Advances in Optimal Transport for Machine Learning,” *IEEE Transactions*

- on *Pattern Analysis and Machine Intelligence*, 2024.
- [17] G. Klambauer, T. Unterthiner, A. Mayr, and S. Hochreiter, “Self-Normalizing Neural Networks,” *Advances in Neural Information Processing Systems (NeurIPS)*, vol. 30, 2017.
- [18] P. Ramachandran, B. Zoph, and Q. V. Le, “Searching for Activation Functions,” *arXiv preprint arXiv:1710.05941*, 2017.
- [19] X. Glorot, A. Bordes, and Y. Bengio, “Deep Sparse Rectifier Neural Networks,” *Proceedings of the 14th International Conference on Artificial Intelligence and Statistics (AISTATS)*, pp. 315–323, 2011.
- [20] W. Shang, K. Sohn, D. Almeida, and H. Lee, “Understanding and Improving Convolutional Neural Networks via Concatenated Rectified Linear Units,” *Proceedings of the 33rd International Conference on Machine Learning (ICML)*, pp. 2217–2225, 2016.
- [21] B. Xu, N. Wang, T. Chen, and M. Li, “Empirical Evaluation of Rectified Activations in Convolutional Network,” *arXiv preprint arXiv:1505.00853*, 2015.
- [22] H. Li, Z. Xu, G. Taylor, C. Studer, and T. Goldstein, “Visualizing the Loss Landscape of Neural Nets,” *Advances in Neural Information Processing Systems (NeurIPS)*, pp. 6391–6401, 2018.
- [23] R. Islamov, N. Ajroldi, A. Orvieto, and A. Lucchi, “Loss Landscape Characterization of Neural Networks without Over-Parametrization,” *arXiv preprint arXiv:2410.12455*, 2024.
- [24] N. S. Keskar, D. Mudigere, J. Nocedal, M. Smelyanskiy, and P. T. P. Tang, “On Large-Batch Training for Deep Learning: Generalization Gap and Sharp Minima,” *arXiv preprint arXiv:1609.04836*, 2016.
- [25] I. Goodfellow, Y. Bengio, and A. Courville, “Deep Learning,” MIT Press, 2016.
- [26] C. Villani, “Optimal Transport: Old and New,” vol. 338, pp. 129–131, *Springer*, Berlin, 2008.
- [27] J. Yosinski, J. Clune, Y. Bengio, and H. Lipson, “How Transferable are Features in Deep Neural Networks?,” *Advances in Neural Information Processing Systems (NeurIPS)*, pp. 3320–3328, 2014.
- [28] K. Simonyan and A. Zisserman, “Very Deep Convolutional Networks for Large-Scale Image Recognition,” *arXiv preprint arXiv:1409.1556*, 2014.
- [29] I. Gulrajani, F. Ahmed, M. Arjovsky, V. Dumoulin, and A. C. Courville, “Improved Training of Wasserstein GANs,” *Advances in Neural Information Processing Systems (NeurIPS)*, vol. 30, 2017.
- [30] A. G. Howard, M. Zhu, B. Chen, D. Kalenichenko, W. Wang, T. Weyand, M. Andreetto, and H. Adam, “MobileNets: Efficient Convolutional Neural Networks for Mobile Vision Applications,” *arXiv preprint arXiv:1704.04861*, 2017.
- [31] M. Lin, Q. Chen, and S. Yan, “Network In Network,” *arXiv preprint arXiv:1312.4400*, 2013.
- [32] A. Krizhevsky, “Learning Multiple Layers of Features from Tiny Images,” University of Toronto, Technical Report, 2009.
- [33] Y. LeCun, L. Bottou, Y. Bengio, and P. Haffner, “Gradient-Based Learning Applied to Document Recognition,” *Proceedings of the IEEE*, vol. 86, no. 11, pp. 2278–2324, 1998.
- [34] H. Xiao, K. Rasul, and R. Vollgraf, “Fashion-MNIST: A Novel Image Dataset for Benchmarking Machine Learning Algorithms,” *arXiv preprint arXiv:1708.07747*, 2017.
- [35] J. Z. Wang, J. Li, and G. Wiederhold, “SIMPLiCity: Semantics-Sensitive Integrated Matching for Picture Libraries,” *IEEE Transactions on Pattern Analysis and Machine Intelligence*, vol. 23, no. 9, pp. 947–963, 2001.

- [36] M. Tan and Q. V. Le, “EfficientNet: Rethinking Model Scaling for Convolutional Neural Networks,” *Proceedings of the 36th International Conference on Machine Learning (ICML)*, pp. 6105–6114, 2019.
- [37] C. Shorten and T. M. Khoshgoftaar, “A Survey on Image Data Augmentation for Deep Learning,” *Journal of Big Data*, vol. 6, no. 1, p. 60, 2019.
- [38] S. H. Gao, M. M. Cheng, K. Zhao, X. Y. Zhang, M. H. Yang, and P. Torr, “Res2Net: A New Multi-Scale Backbone Architecture,” *IEEE Transactions on Pattern Analysis and Machine Intelligence*, vol. 43, no. 2, pp. 652–662, 2019.
- [39] P. S. Hiremath and J. Pujari, “Content Based Image Retrieval Using Color, Texture and Shape Features,” in *Proceedings of the 15th International Conference on Advanced Computing and Communications (ADCOM)*, pp. 780–784, IEEE, 2007.
- [40] C. Zhang, S. Bengio, M. Hardt, B. Recht, and O. Vinyals, “Understanding Deep Learning Requires Rethinking Generalization,” *arXiv preprint arXiv:1611.03530*, 2016.
- [41] B. Neyshabur, S. Bhojanapalli, D. McAllester, and N. Srebro, “Exploring Generalization in Deep Learning,” *Advances in Neural Information Processing Systems (NeurIPS)*, vol. 30, 2017.
- [42] K. Kawaguchi, “Deep Learning Without Poor Local Minima,” *Advances in Neural Information Processing Systems (NeurIPS)*, vol. 29, 2016.
- [43] D. Kingma and J. Ba, “Adam: A Method for Stochastic Optimization,” *arXiv preprint arXiv:1412.6980*, 2014.
- [44] I. Loshchilov and F. Hutter, “Decoupled Weight Decay Regularization,” *arXiv preprint arXiv:1711.05101*, 2017.
- [45] A. Shakarami, Y. Yeganeh, A. Farshad, L. Nicolè, S. Ghidoni, and N. Navab, “Stress-Aware Resilient Neural Training,” *arXiv preprint arXiv:2508.00098*, 2025.
- [46] A. Shakarami, L. Nicolè, R. Cappellesso, A. P. Dei Tos, and S. Ghidoni, “DepViT-CAD: Deployable Vision Transformer-Based Cancer Diagnosis in Histopathology,” *arXiv preprint arXiv:2507.10250*, 2025.
- [47] A. Shakarami, M. B. Menhaj, A. Mahdavi-Hormat, and H. Tarrah, “A Fast and Yet Efficient YOLOv3 for Blood Cell Detection,” *Biomedical Signal Processing and Control*, vol. 66, p. 102495, 2021.
- [48] A. Shakarami, L. Nicolè, M. Terreran, A. P. Dei Tos, and S. Ghidoni, “TCNN: A Transformer Convolutional Neural Network for Artifact Classification in Whole Slide Images,” *Biomedical Signal Processing and Control*, vol. 84, p. 104812, 2023.
- [49] A. Shakarami, H. Tarrah, and A. Mahdavi-Hormat, “A CAD System for Diagnosing Alzheimer’s Disease Using 2D Slices and an Improved AlexNet-SVM Method,” *Optik*, vol. 212, p. 164237, 2020.
- [50] A. Shakarami, M. B. Menhaj, and H. Tarrah, “Diagnosing COVID-19 Disease Using an Efficient CAD System,” *Optik*, vol. 241, p. 167199, 2021.
- [51] A. Shakarami, A. Farshad, Y. Yeganeh, L. Nicolè, P. Schuffler, S. Ghidoni, and N. Navab, “UNIT-Based Histopathology Tissue Segmentation via Multi-Level Feature Representation,” *arXiv preprint arXiv:2507.12427*, 2025.
- [52] A. Shakarami *et al.*, “Transformative AI for Automating Histopathology Workflows,” Università degli Studi di Padova, 2025.
- [53] G. Litjens, T. Kooi, B. Bejnordi, A. Setio, F. Ciompi, M. Ghafoorian, ... and J. van der Laak, “A Survey on Deep Learning in Medical Image Analysis,” *Medical Image Analysis*, vol. 42, pp. 60–88, 2017.
- [54] D. Shen, G. Wu, and H. Suk, “Deep Learning in Medical Image Analysis,” *Annual Review*

- of *Biomedical Engineering*, vol. 19, pp. 221-248, 2017.
- [55] A. Howard, M. Sandler, G. Chu, L.-C. Chen, B. Chen, M. Tan, ... and H. Adam, "Searching for MobileNetV3," *Proceedings of the IEEE International Conference on Computer Vision (ICCV)*, pp. 1314-1324, 2019.
- [56] J. Deng, W. Dong, R. Socher, L. Li, K. Li, and L. Fei-Fei, "ImageNet: A Large-Scale Hierarchical Image Database," *Proceedings of the IEEE Conference on Computer Vision and Pattern Recognition (CVPR)*, pp. 248-255, 2010.
- [57] Y. Bengio, "Practical Recommendations for Gradient-Based Training of Deep Architectures," *Neural Networks: Tricks of the Trade*, pp. 437-478, 2012.
- [58] J. Bergstra and Y. Bengio, "Random Search for Hyper-Parameter Optimization," *Journal of Machine Learning Research*, vol. 13, pp. 281-305, 2012.
- [59] M. Feurer and F. Hutter, "Hyperparameter Optimization," *Automated Machine Learning*, pp. 3-33, 2019.
- [60] L. Li, K. Jamieson, G. DeSalvo, A. Ros-tamizadeh, and A. Talwalkar, "Hyperband: A Novel Bandit-Based Approach to Hyperparameter Optimization," *Journal of Machine Learning Research*, 2017.
- [61] J. Bergstra, R. Bardenet, Y. Bengio, and B. Kégl, "Algorithms for Hyper-Parameter Optimization," *Advances in Neural Information Processing Systems (NeurIPS)*, 2011.
- [62] J. Snoek, H. Larochelle, and R. P. Adams, "Practical Bayesian Optimization of Machine Learning Algorithms," *Advances in Neural Information Processing Systems (NeurIPS)*, 2012.
- [63] C. Finn, P. Abbeel, and S. Levine, "Model-Agnostic Meta-Learning for Fast Adaptation of Deep Networks," *Proceedings of the International Conference on Machine Learning (ICML)*, 2017.
- [64] T. Akiba, S. Sano, T. Yanase, T. Ohta, and M. Koyama, "Optuna: A Next-generation Hyperparameter Optimization Framework," *Proceedings of the ACM SIGKDD International Conference on Knowledge Discovery and Data Mining*, 2019.
- [65] J. Bergstra, D. Yamins, and D. Cox, "Making a Science of Model Search: Hyperparameter Optimization in Hundreds of Dimensions for Vision Architectures," *Proceedings of the International Conference on Machine Learning (ICML)*, 2013.
- [66] T. O'Malley, E. Bursztein, L. Long, F. Chollet, H. Jin, and others, "Keras Tuner," *GitHub repository*, 2019.
- [67] J. Yang, R. Shi, D. Wei, Z. Liu, L. Zhao, B. Ke, H. Pfister, and B. Ni, "MedMNIST v2: A Large-Scale Lightweight Benchmark for 2D and 3D Biomedical Image Classification," *Scientific Data*, vol. 10, no. 1, p. 41, 2023.
- [68] Y. Zhang, K. Gong, X. Ding, K. Zhang, F. Lv, K. Keutzer, and X. Yue, "Towards Unified and Effective Domain Generalization," *arXiv preprint arXiv:2310.10008*, 2023.
- [69] S. Li, Z. Liu, Z. Wang, D. Wu, Z. Liu, and S. Z. Li, "Boosting Discriminative Visual Representation Learning with Scenario-Agnostic Mixup," *arXiv preprint arXiv:2111.15454*, 2021.
- [70] P. Helber, B. Bischke, A. Dengel, and D. Borth, "EuroSAT: A Novel Dataset and Deep Learning Benchmark for Land Use and Land Cover Classification," *IEEE Journal of Selected Topics in Applied Earth Observations and Remote Sensing*, vol. 12, no. 7, pp. 2217-2226, 2019.
- [71] E. D. Cubuk, B. Zoph, D. Mane, V. Vasudevan, and Q. V. Le, "AutoAugment: Learning Augmentation Policies from Data," *arXiv preprint arXiv:1805.09501*, 2018.
- [72] K. He, X. Zhang, S. Ren, and J. Sun, "Delving Deep into Rectifiers: Surpassing Human-Level Performance on ImageNet Classification," *Proceedings of the IEEE International Conference on Computer Vision (ICCV)*, pp. 1026-1034, 2015.

- [73] Y. Chen, X. Dai, M. Liu, D. Chen, L. Yuan, and Z. Liu, “Dynamic ReLU,” in *Proceedings of the European Conference on Computer Vision (ECCV)*, pp. 351–367, Springer, Cham, 2020.
- [74] S. Ruder, “An Overview of Gradient Descent Optimization Algorithms,” *arXiv preprint arXiv:1609.04747*, 2016.
- [75] G. Hinton, N. Srivastava, and K. Swersky, “Neural Networks for Machine Learning: Lecture 6a – Overview of Mini-Batch Gradient Descent,” unpublished lecture notes, University of Toronto, 2012.